Journal of
8/15

BIOPHOTONICS

www.biophotonics-journal.org

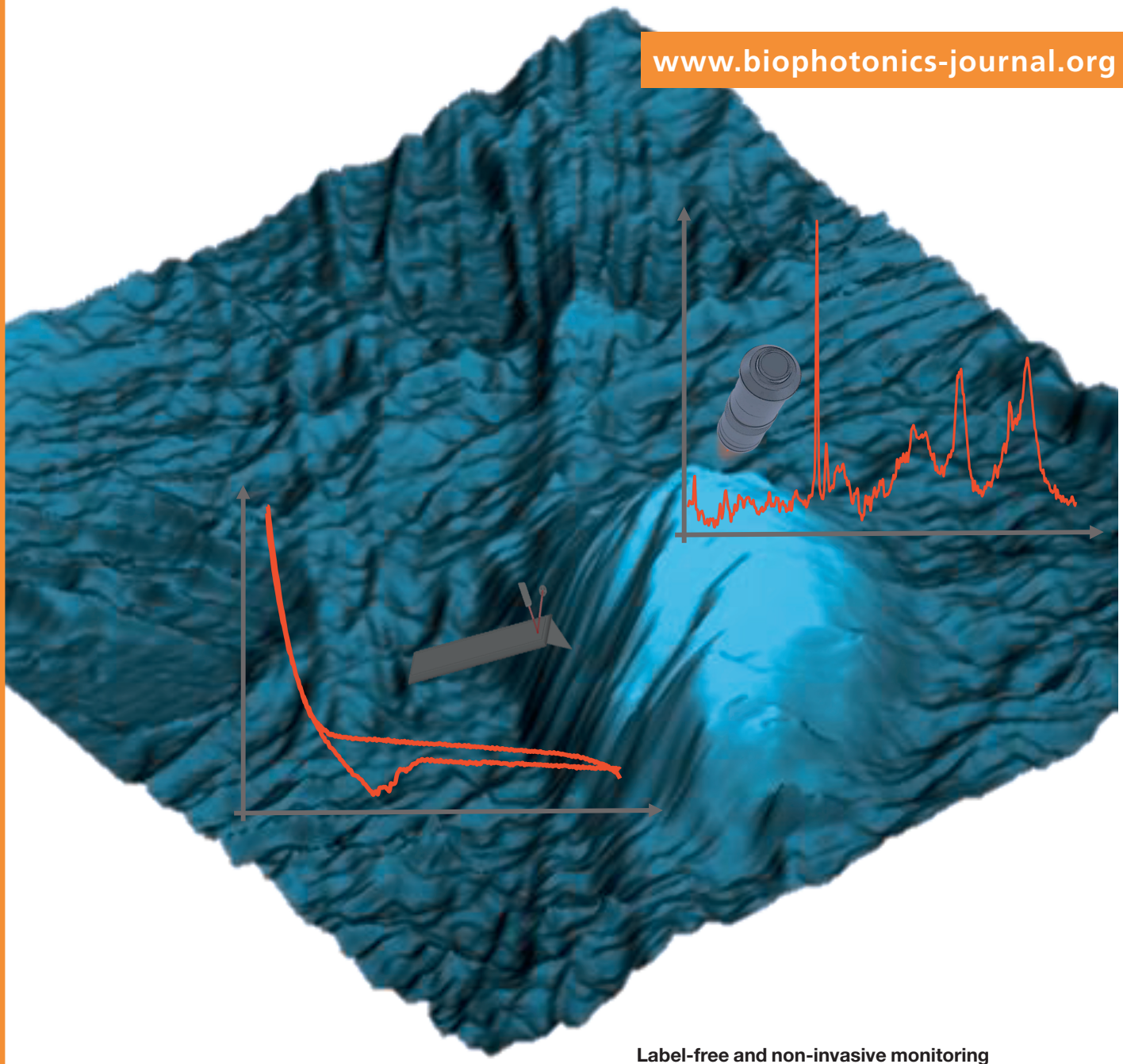

Label-free and non-invasive monitoring of porcine trophoblast derived cells: differentiation in serum and serum-free media
Qifei Li, Edison Suasnavas, Lifu Xiao, Sierra Heywood, Xiaojun Qi, Anhong Zhou, and S. Clay Isom

WILEY-VCH
ISSN 1864-0648 J. Biophotonics, Vol. **8**, No. 8 (August), 611–687 (2015)

J. Biophotonics **8**, No. 8, 638–645 (2015) / **DOI** 10.1002/jbio.201400062

Journal of BIOPHOTONICS

FULL ARTICLE

Label-free and non-invasive monitoring of porcine trophoblast derived cells: differentiation in serum and serum-free media

*Qifei Li***, [1], *Edison Suasnavas***, [2], *Lifu Xiao*[1], *Sierra Heywood*[2], *Xiaojun Qi*[3], *Anhong Zhou**, [1], *and S. Clay Isom**, [2]

[1] Department of Biological Engineering, Utah State University, Logan, UT 84322
[2] Department of Animal Science, Dairy and Veterinary Sciences, Utah State University, Logan, UT 84322
[3] Department of Computer Science, Utah State University, Logan, UT 84322

Received 6 June 2014, revised 3 August 2014, accepted 27 August 2014
Published online 23 August 2014

Key words: Raman microspectroscopy, principal component analysis (PCA), atomic force microscopy (AFM), qPCR, transfected porcine trophoblast derived cells, cellular differentiation

Traditional approaches to characterize stem cell differentiation are time-consuming, lengthy and invasive. Here, Raman microspectroscopy (RM) and atomic force microscopy (AFM) – both considered as non-invasive techniques – are applied to detect the biochemical and biophysical properties of trophoblast derived stem-like cells incubated up to 10 days under conditions designed to induce differentiation. Significant biochemical and biophysical differences between control cells and differentiated cells were observed. Quantitative real time PCR was also applied to analyze gene expression. The relationship between cell differentiation and associated cellular biochemical and biomechanical changes were discussed.

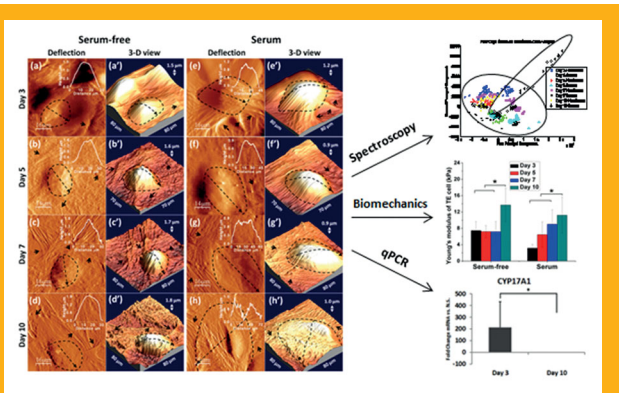

Monitoring trophoblast cells differentiation

1. Introduction

In vitro characterization of cellular differentiation using traditional methods, including immunocytochemistry, fluorescence activated cell sorting and RNA in situ hybridization analysis, has limitations: all require large numbers of cells, lengthy steps and cellular lysis or fixation [1–3]. Recently, there has been a drive to characterize and monitor cellular differentiation processes in situ and real-time by faster and non-invasive methods. Raman microspectroscopy (RM) and atomic force microscopy (AFM) are two highly sensitive analytical techniques able to characterize cellular biochemical [4] and biomecha-

* Corresponding authors: e-mail: Anhong.Zhou@usu.edu, Phone: +1 435 797 2863, Fax: +1 435 797 1248; Clay.Isom@usu.edu
** These authors contributed equally to this work.

nical [5] properties in cell samples under near physiological conditions [6].

RM is a spectroscopic technique based on inelastic scattering that exhibits energy shift of laser photons corresponding to frequencies of vibration within molecules from samples. Raman shifts can serve as a "fingerprint" to provide information about the molecular compositions, structures, and quantities of cellular biopolymers with a minimal background signal from water [7, 8], allowing the study of living cells under physiological states, without labels or using other invasive steps [9]. Previous studies reported that Raman intensities of nucleic acids on undifferentiated stem cells were dominant in comparison with differentiated cells, while differentiated cells had larger spectral intensities of proteins and lipids than undifferentiated cells [6, 7, 10–18].

AFM is a high-resolution scanning probe microscopy that involves the movement of a sharp tip over the surface of a biological sample while detecting the near-field physical interactions between the sample and tip [19, 20]. AFM can image cytoskeleton, cellular microenvironments, and quantitatively detect cellular mechanical properties at nanometer scales in physiological condition [5, 21, 22]. It was found that stem cell stiffness will increase with differentiation [23–25] and cellular mechanical properties are indicative of stem cell differentiation potential [26, 27].

In the earliest stages of eutherian mammalian embryo development, all the cells (blastomeres) are functionally equivalent, and equally capable of giving rise to all cell types necessary for proper and complete embryonic/fetal growth and survival. However, at a species-specific timepoint (approximately day 3 in mice, day 5 in humans and pigs, and day 7 in cattle, e.g.), molecular and morphological transitions destine some of the cells for development into the primitive placenta (i.e. the trophectoderm), while the remaining cells give rise to the embryo/fetus proper (i.e. the so-called embryonic stem cells) and retain a relatively undifferentiated status [28–30]. Trophoblast cells are the first cells within the early developing embryo to undergo a recognizable differentiation event, and the proper formation and function of cells is essential to embryo and fetal survival. In fact, many instances of early embryo mortality – at least in in vitro-manipulated embryos – can be traced back to dysfunctional trophoblast cells [31–33]. Yet the process of trophoblast differentiation is poorly understood. A thorough appreciation of the biochemical and biophysical aspects of trophoblast differentiation may enhance trophoblast function for increased embryonic survival.

In this experiment, trophoblast stem-like cells derived from day 10 porcine embryos have been induced by serum and serum-free medium to study cellular differentiation in physiological conditions. This is the first work to combine RM and AFM to monitor and identify discrete biochemical and biomechanical changes during serum-induced differentiation.

2. Experimental

2.1 Preparation of trophoblast cells

The cells were collected from porcine embryos on gestational day 10 as described elsewhere (Suasnavas et al., unpublished) and were passaged without senescence or morphological changes until utilized for experiments. Cell colonies were transfected with an expression construct coding for green fluorescent protein (GFP) using Jet Pei reagent (Polyplus transfection Inc., NY, USA) according to instructions. GFP cells help observe TE cells morphological changes on magnesium fluoride (MgF_2, United Crystals Co., Port Washington, NY, USA) over time without chemical label. Cells were cultured in serum-free medium to maintain undifferentiated, stem-like characteristics [34], whereas cells cultured in fetal bovine serum medium (15% [v:v]) underwent dramatic and predictable changes to cell morphology and behavior (data not shown here; manuscript in preparation). Table S1 lists formulations for serum-free and serum-containing medium.

2.2 Fluorescence imaging of trophoblast cells

Bright field and fluorescence images were collected by Olympus IX71 inverted fluorescence microscope (Olympus America Inc., USA) equipped with an Olympus DP30BW CCD camera using DP-BSW Controller and Manager Software. Images were acquired via a 10× lens (Olympus), and cell samples grown on MgF_2 substrates were observed in medium. Fluorescence images were processed by ImageJ software and nucleus diameter measurements were performed on 50~100 cells.

2.3 Raman microspectroscopy

The Raman spectra were measured by Renishaw inVia Raman spectrometer (WiRE 3.0 software, Renishaw, UK) equipped with a 300 mW 785 nm near-IR laser that was focused through a 63 × (NA = 0.90) water immersion objective (Leica Microsystems, USA). Cells were cultured on MgF_2 and im-

aged in Earle's balanced salt solution (EBSS, Invitrogen).

The Raman laser spot size is about 24 μm × 0.5 μm, focusing primarily on the cellular nuclear region. Raman spectra were collected at Raman static mode at 1 accumulation with 10 s exposure time. At each treatment group, two MgF_2 windows with cells were measured. On each treatment group, 40 ~ 60 Raman spectra from multiple individual cells (10 ~ 15 cells, each cell collected 4 spectra) were detected within 2 hours at room temperature. Renishaw Wire 3.3 software performed for Raman spectra baseline corrected, spectral smoothed and normalized at maximum peaks. The processed spectra were imported to OriginPro 8 software (OriginLab Corp., MA, USA) for Raman intensity analysis. The significance testing was employed by one-way ANOVA, and the data were reported as mean ± SD. PCA was processed in Matlab R2012b using baseline corrected data.

2.4 Atomic Force Microscopy

Contact mode AFM controlled by Picoview software (Picoplus, Agilent Technologies) was applied to trophoblast cells on MgF_2 in culture medium. Sharp silicon nitride AFM probes (tip radius, 20 nm) were employed (Bruker Corp., Billerica, MA, USA). Spring constant of tips was calibrated as 0.10 ~ 0.11 N/m and deflection sensitivities were 45 ~ 50 nm/V.

Scanning Probe Image Processor (SPIP) software (Image Metrology, Denmark) calculated Young's modulus by converting the force-distance curves to force-separation curves and fitting the Sneddon variation of Hertz model as below formula shows [35–37]:

$E_{cell} = 4 \cdot F_{(\Delta Z)} \cdot (1 - \eta_{cell}^2)/3 \cdot (\Delta Z^{1.5}) \cdot \tan\theta$, where E_{cell}: Young's modulus; F: loading force; η_{cell}: Poisson ratio; ΔZ: indentation; θ: tip half cone opening angle.

The Poisson's ratio was 0.5 and the tip half cone opening angle was 36°. For each group, at least 20 force curves of each cell (the total cells are over 15) were collected, and detection was accomplished within 2 hours to approximate normal physiologic conditions. The AFM images were processed with WSXM software (Nanotec, Madrid, Spain) for deflection and 3-D view.

2.5 Quantitative real time PCR analysis

On days 3 and 10, total RNA was isolated from cells by the Total RNA kit I (Omega Bio-tek; Norcross, GA) following protocol. mRNA was reverse transcribed using GoScript Reverse Transcription System kit from Promega (Madison, WI). Quantitative PCR (qPCR) was performed on the Eppendorf Mastercylcer Realplex2 machine using Promega GoTaq qPCR master mix with primers (Table S2) for HAND1, KLF4, CYP17A1, KRT8 and EIF4A1 genes.

3. Results and discussion

3.1 Fluorescence imaging for trophoblast cells

Figure 1 compares nucleus diameter of the groups at different days (Figure 1(a)) and shows representative cell images on each group (Figure 1(b)). Figure S1 displays the histogram of cell nucleus diameter at day 3, 5, 7 and 10 in serum-free and serum medium. According to Figure 1(a), the nucleus diameter of serum-free cell maintains similar value with time,

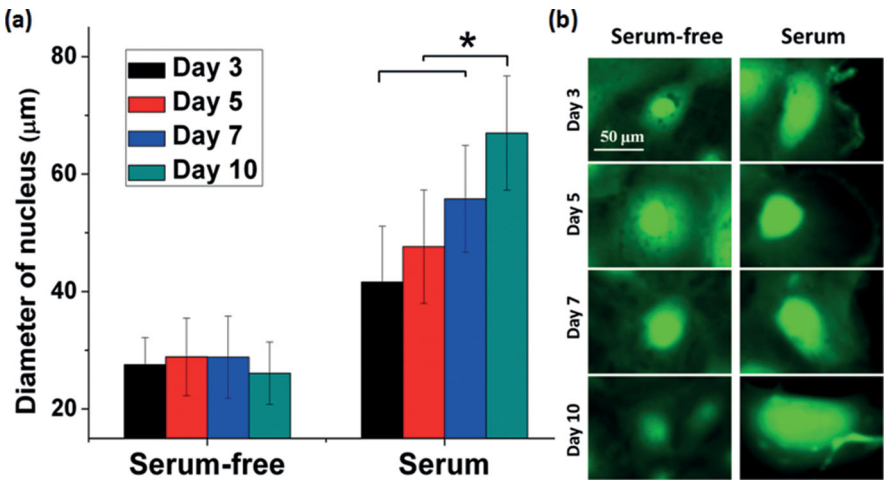

Figure 1 Nucleus diameter of trophoblast cells (**a**) and representative GFP images of cells in serum-free and serum medium at day 3, 5, 7 and 10 (Error bars of (**a**) are standard deviation of the mean (each bar has at least 50 samples), *means $P < 0.05$).

from 27.5 ± 4.6 μm at day 3 to 26.1 ± 5.3 μm at day 10. On the contrary, the nucleus diameter of cells in serum gradually increases with time, from 41.6 ± 9.5 μm at day 3 to 55.8 ± 9.1 μm at day 7, maximizing at day 10 (67.0 ± 9.7 μm). Figure S2 shows that cells grown in serum medium exhibit larger cell shape with less proliferative feature over time, compared with those in serum-free medium at the same date.

Overall, the above observations indicate trophoblast cells maintain smaller nucleus diameter in serum-free medium up to 10 days.

3.2 *Raman intensity comparison*

After exposure to 785 nm laser in Raman detection (within 2 hrs), LIVE/DEAD Viability/Cytotoxicity was conducted by staining cells with Calcein AM (green, live cells)/ethidium homodimer-1 (red, dead cells) (Invitrogen). Few dead cells were observed as shown in Figure S3, indicating little photodamage effect from near infrared light, which is consistent with previous studies [38–40]. Comparing GFP and non-GFP cells in Figure S4, there is ignorable difference in Raman spectra. Thus, GFP-TE cells were used in this work for better morphological observation.

Table S3 lists the tentative Raman band assignments of trophoblast cells. Averaged Raman spectra of different groups are shown in Figure S5. There are some remarkable differences among groups, for example, 717 cm^{-1} CN–$(CH_3)_3$ (lipid/choline)), 760 cm^{-1} (Tryptophan), 786 cm^{-1} (DNA & phosphdiester bands DNA), 813 cm^{-1} (Phosphodiester bands RNA), 1006 cm^{-1} (Phenylalanine) and 1057 cm^{-1} (lipid). The mean Raman peaks intensities were extracted to quantitatively analyze the differences, as shown in Figure 2. For serum groups, the DNA intensity gradually decreases from 0.12 at day 3 to 0.09 at day 10 (Figure 2(a)). However, the DNA intensity of cells in serum-free medium fluctuates over time. Similar to DNA changes, the RNA intensity of serum groups (Figure 2(b)) slowly drops, while that of cells in serum-free medium fluctuates over times. The tryptophan (760 cm^{-1}) intensity of serum groups (Figure 2(c)) increases over time. However, for cells in serum-free medium the tryptophan intensity fluctuates. Similarly, for serum groups the phenylalanine (1006 cm^{-1}) intensity (Figure 2(d)) grows continuously, while that of cells in serum-free medium fluctuates with time. The lipid/choline intensities (717 cm^{-1} and 1057 cm^{-1}) fluctuates with time regardless cells in serum or serum-free medium (Figure 2(e–f)).

Our spectral results are similar to previous studies [10, 38, 41, 42] that an increase of protein peak

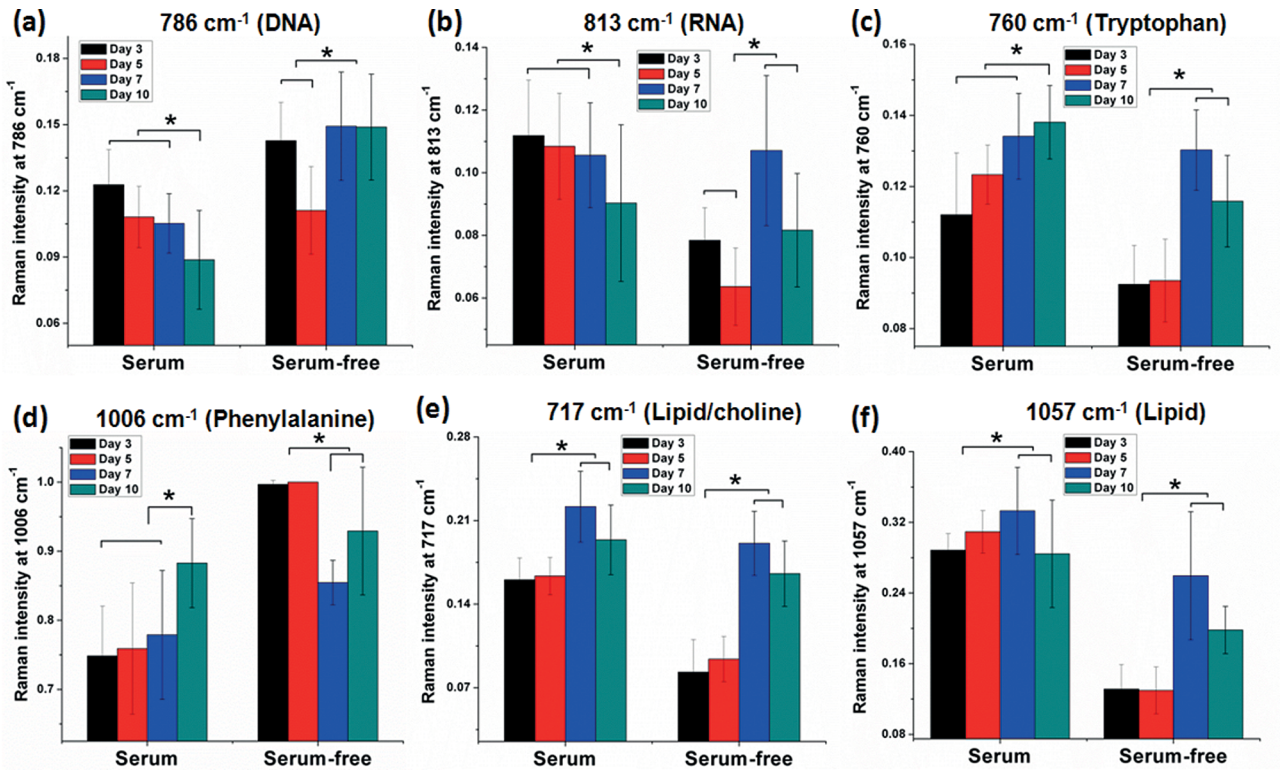

Figure 2 Raman peak intensity analysis of trophoblast cells on DNA (a), RNA (b), tryptophan (c), phenylalanine (d), lipid/choline (e) and lipid (f) at day 3 (black), 5 (red), 7 (blue) and 10 (cyan) in serum and serum-free medium (Error bars (each bar has at least 40 samples) are standard deviation of the mean, * means $P < 0.05$).

intensity and decrease of nucleic acids peak intensity are related to the differentiation of stem cells. However, the lipid peak intensities exhibits an increasing trend. Regardless of the days in culture, the lipid peaks of serum groups (differentiated cells) are higher than those of serum-free groups (undifferentiated cells). The lipid peaks do not show a steady increase in trophoblast cell system, which is not consistent with those observation in multipotent and pluripotent stem cells [13]. The reason may be accounted for different cell types and different culture conditions.

3.3 Spectroscopic markers comparison and principal component analysis of Raman spectra

Previous studies indicate increasing 757 cm^{-1} to 784 cm^{-1} intensity ratio is correlated with the reduction of *Oct4* and *Nanog* expression, which decrease rapidly with the differentiation of human embryonic stem cells (hESCs) [38, 43] and human induced pluripotent stem cells (hiPSCs) [44]. Here, the peak intensity ratio of 760 cm^{-1} (tryptophan) to 786 cm^{-1} (DNA) was applied to assess trophoblast cells differentiation.

Peak intensity ratio (760 cm^{-1}/786 cm^{-1}) of trophoblast cells are presented in Figure 3(a) (inset fluorescence images of cells at day 10). The ratios in serum medium were larger than those in serum-free medium at each day. For serum groups the ratio increase in the first five days, then drops slightly, reaching the maximum at day 10. The ratio of serum-free groups grows in the first seven days, then decrease largely at day 10. This ratio of serum groups increased with time, probably suggesting the cellular differentiation. In contrast, the ratio fluctuated for serum-free groups, which may indicate cells still remain undifferentiated or differentiated slowly in serum-free medium.

Turner et al. have successfully assessed hESCs differentiation by distribution diagram of two protein/nucleic acid intensity ratios (757 cm^{-1}/784 cm^{-1} (tryptophan/nucleic acid) and 853 cm^{-1}/784 cm^{-1} (tyrosine/nucleic acid)) [38]. We applied the same method as shown in Figure 3(b). The X-axis displays the peak intensity ratio of 760 cm^{-1}/786 cm^{-1}, and Y-axis is the peak intensity ratio of 854 cm^{-1}/786 cm^{-1}. The serum group at day 10 (upper right) has the largest distribution in comparison with other groups, even though over 50% of these points overlay with other points.

Principal component analysis (PCA) is also applied to analyze Raman spectra difference for serum and serum-free groups (each group has ≈ 200 spectra). PCA simplifies the spectra by exhibiting the data with principal component (PC) variables ordered from the largest variance to the least variance [45]. The X-axis and Y-axis correspond to the 1st and the 2nd PC variables, respectively. Figure S6 presents the calculated loading vectors of the first PC and the second PC, i.e., PC1 and PC2. These two PCs account for 87.58% of variance and mainly represent the Raman spectra of the cells. Similarly to Figure 3(b), the data points in serum group at day 10 (white diamond) are not closely clustered, even over 50% of these points overlay with other groups as shown in Figure 3(c). Clusters of other groups sit tightly with each other.

Our distribution diagram and PCA analysis (Figure 3(b, c)) both imply that "Day 10 serum" group exhibits the largest distribution of cellular biocomponents (e.g., proteins/nucleic acids) among other groups.

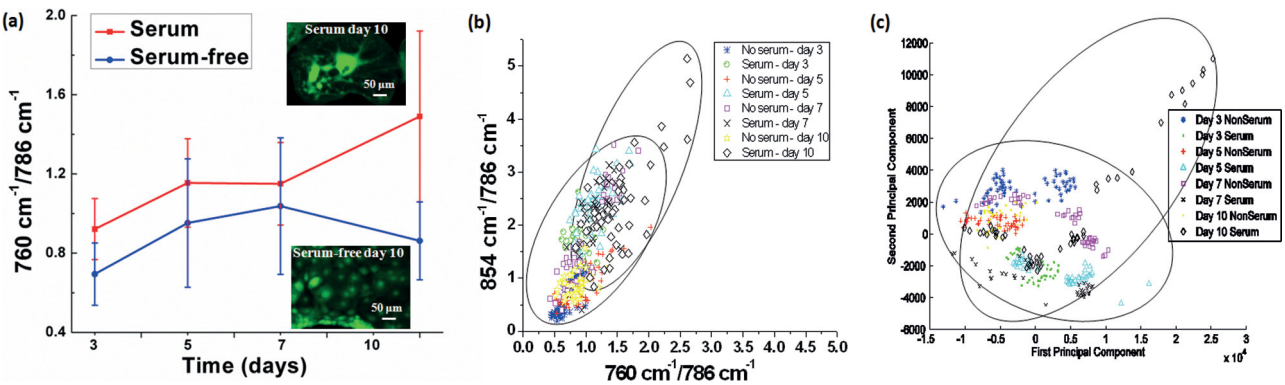

Figure 3 Raman peak ratio (760 cm^{-1}/786 cm^{-1}) in serum and serum-free medium (**a**) (Inset fluorescence images of trophoblast cells at day 10, scale bar: 50 μm); distribution diagram of two protein/nucleic acid peak intensity ratios (760/786 cm^{-1} and 854/786 cm^{-1}) (**b**), and PCA plot (**c**) (Error bars of (**a**) are standard deviation of the mean (each bar has at least 40 samples), * means $P < 0.05$).

3.4 Topography and biomechanics comparison

The nucleus diameter can be obtained by AFM, as shown in Figure 4. The inset is the line profiling of nucleus height crossed cells. The nucleus diameter of cells in serum-free medium (Figure 4 (a–d, a′–d′)) remains the similar value over time, while its cytoskeleton structures (e.g., filamentous actin bundles) increase from over time. However, the nucleus diameter of serum group (Figure 4 (e–h, e′–h′)) increases with time, and its surrounding cytoskeleton structures become less visible over time. At day 3, mesh-like structures are clearly visible on surface of cells in serum (Figure 4 (e, e′) black arrows pointed) in comparison with those of serum-free group (Figure 4(a, a′) one black arrow pointed). Meantime, the nucleus diameter (~42 μm) of cells in serum medium is larger than that (~27 μm) of cells in serum-free medium. At day 5, the nucleus diameter (~32 μm) of cells in serum-free medium is still less than that (48 μm) of cells in serum medium. Similar trends are observed over 7 days (cells in serum medium have larger nucleus diameter than those in serum-free medium). For the height differences, the overall height (around 1.65 μm) of cells in serum-free medium is higher than that (around 1.00 μm) of cells in serum medium over time. The AFM image analysis confirms the result of nucleus diameter shown in Figure 1.

To analyze the biomechanics properties, we compare the Young's modulus (via AFM force-distance curve measurements) of different groups (Figure 5). Serum groups show a gradual increase in Young's modulus over time, from 3.16 ± 0.90 kPa at day 3 to 11.20 ± 4.41 kPa at day 10. However, Young's modulus of serum-free groups remains unchanged (~7.30 kPa) from day 3 to 7, then significantly increases to 13.70 ± 4.11 kPa at day 10.

The Young's modulus gradually increases in serum groups over time, which is similar to the mouse embryonic stem cells study conducted by Pillarisetti et al. [24]. However, that of serum-free groups maintains stable at first 7 days, followed by significant increase at day 10. Further studies are needed to investigate the reason leading to Young's modulus increase of undifferentiated cells at day 10.

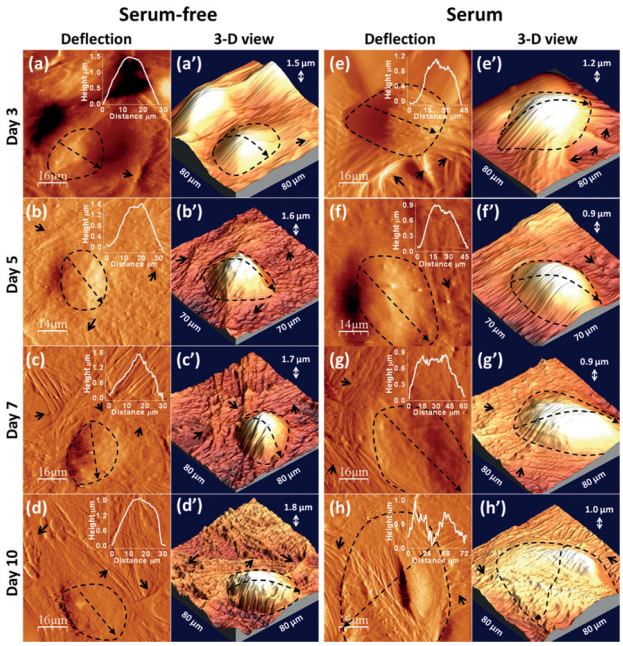

Figure 4 AFM deflection (**a–h**) and corresponding 3-D view (**a′–h′**) images of cells in serum-free and serum medium at day 3, 5, 7 and 10. Insets in deflection images are the line profiling of nucleus height.

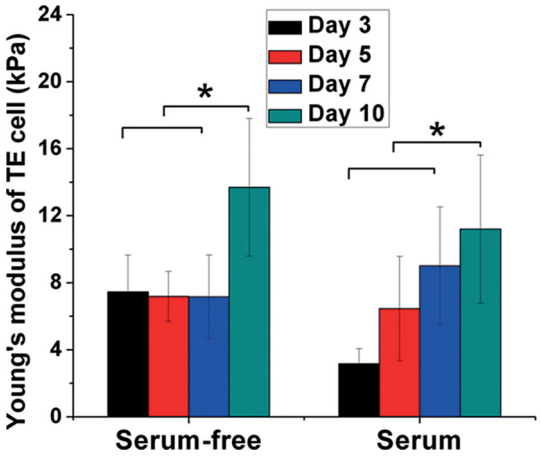

Figure 5 Young's modulus of cells in serum-free and serum medium at day 3, 5, 7 and 10. Error bars (each bar has at least 200 samples) are standard deviation of the mean, *means $P < 0.05$.

3.5 Analysis of gene expression by qPCR

Four genes were selected for qPCR: CYP17A1, HAND1, KLF4 and KRT8. The gene CYP17A1 is involved in the steroid biosynthetic pathway, testing for differentiation [46]. HAND1 is essential for placental development and to promote trophoblast giant cells differentiation [47]. The KLF4 gene is a transcription factor that regulates proliferation, differentiation, development and apoptosis [48]. KRT8 is prominent in simple single-layer epithelial cells, such as differentiated trophoblast [49].

In Figure 6, the X-axis displays time point and the Y-axis shows the expression ratio (fold-change; serum/non-serum). Figure 6(a) exhibits that on day 3 CYP17A1 are approximately 200-fold higher for serum group than serum-free group, but this discrepancy has disappeared by day 10. Day 3 HAND1 from serum-treated cells are undetectable, thus there is insufficient data (N/A = not available) in Panel B.

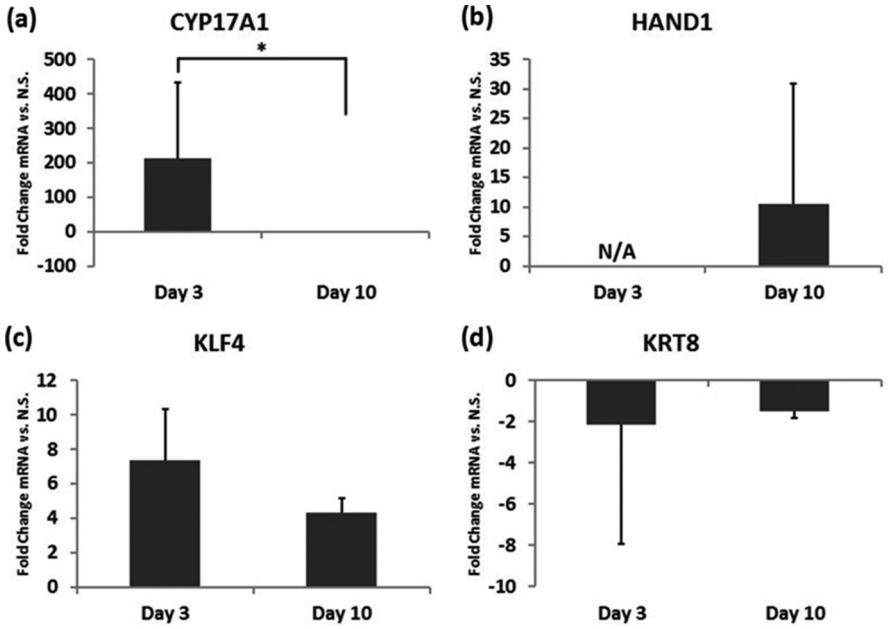

Figure 6 Gene expression analysis of cells cultured 3 and 10 days in serum medium compared to serum-free medium by qPCR. All values are presented as a ratio of fold-change values: Serum/Non-serum fold-change. (**a**) CYP17A1 levels. The ratio at day 10 was approach zero, which does not register on the scale used to present the data, but should not be interpreted as an absent or null value (as in panel b); (**b**) HAND1 levels; (**c**) KLF4 levels; (**d**) Relative KRT8 levels. Error bars are standard error of the mean. (* means $P < 0.05$; N.S. = non-serum; N/A = fold change ratio not available because of a null value for non-serum group).

Panel C shows there is a numerical drop in relative KLF4 gene expression in serum- vs. un-treated cells, but this drop is not statistically significant and relative KRT8 gene expression levels do not change significantly across time in Panel D.

Cells express very low levels of CYP17A1 when cultured in serum-free conditions, but CYP17A1 is turned on when these cells are in serum medium. After three days the cells in serum medium showed a 200 fold upregulation of CYP17A1 compared to the serum-free groups. There is a significant decrease of CYP17A1 from day 3 to day 10. HAND1 transcripts were undetectable in serum groups on day 3, so expression ratio was not feasible. For day 10, the serum group had 12-fold higher HAND1 expression compared to the cells cultured in non-serum medium, which is consistent with the role played by HAND1 in cellular differentiation. qPCR results demonstrated a non-significant drop when analyzing KLF4 and KRT-8 genes. Thus, these genes might not have an impact on these cells. The medium and time differences might impact the expression of certain genes, and these biomacromolecules variations can also be observed in Figure 2.

Our initial qPCR results give us clues that we may seek and screen more genes related to cell biomechanics (e.g., cell adhesion, extracellular matrix) and cell differentiation to sort out such potential correlation.

4. Conclusion

Porcine trophoblast derived cells are interesting model for stem like cell research for their regenerative properties, indefinite passage, and foreign DNA receptivity. Trophoblast cells exhibit different morphologies and functions with/without serum medium, providing a unique tool for studying trophoblast cell differentiation. This is the first work to combine RM and AFM to compare trophoblast cell differentiation, showing that RM and AFM are able to distinguish between undifferentiated and differentiated trophoblast cells. Meantime, this work evaluated the biochemical and biophysical changes of both undifferentiated and differentiating cells at the same day instead of only studying cellular differentiation over time. Characterization of trophoblast cells biochemical and biophysical properties extends the knowledge to further investigations as this area develops.

Supporting Information

Additional supporting information can be found in the online version of this article at the publisher's website: doi: http://dx.doi.org/10.1002/jbio.201400062.

Acknowledgements We thank the support from Utah Agriculture Experiment Station (A.Z. and C.I.). Q. Li also thanks the support from China Scholarship Council (CSC).

Author biographies Please see Supporting Information online.

References

[1] A. Leahy, J. W. Xiong, F. Kuhnert, and H. Stuhlmann, J Exp Zool **284**, 67–81 (1999).
[2] J. Alcock and V. Sottile, Cell research **19**, 1324–1333 (2009).
[3] E. Ratcliffe, R. J. Thomas, and D. J. Williams, British medical bulletin **100**, 137–155 (2011).
[4] M. Tang, Q. Li, L. Xiao, Y. Li, J. L. Jensen, T. G. Liou, and A. Zhou, Toxicol Lett **215**, 181–192 (2012).
[5] Y. Z. Wu, G. D. McEwen, S. Harihar, S. M. Baker, D. B. DeWald, and A. H. Zhou, Cancer Lett **293**, 82–91 (2010).
[6] A. Ghita, F. C. Pascut, M. Mather, V. Sottile, and I. Notingher, Anal Chem **84**, 3155–3162 (2012).
[7] J. W. Chan and D. K. Lieu, J Biophotonics **2**, 656–668 (2009).
[8] A. Zoladek, F. C. Pascut, P. Patel, and I. Notingher, J Raman Spectrosc **42**, 251–258 (2011).
[9] I. Notingher and L. L. Hench, Expert Rev Med Devic **3**, 215–234 (2006).
[10] L. Notingher, I. Bisson, J. M. Polak, and L. L. Hench, Vib Spectrosc **35**, 199–203 (2004).
[11] A. Downes, R. Mouras, and A. Elfick, J Biomed Biotechnol, DOI: Artn 101864 Doi 10.1155/2010/101864 (2010).
[12] H. K. Chiang, F. Y. Peng, S. C. Hung, and Y. C. Feng, J Raman Spectrosc **40**, 546–549 (2009).
[13] J. K. Pijanka, D. Kumar, T. Dale, I. Yousef, G. Parkes, V. Untereiner, Y. Yang, P. Dumas, D. Collins, M. Manfait, G. D. Sockalingum, N. R. Forsyth, and J. Sule-Suso, Analyst **135**, 3126–3132 (2010).
[14] F. C. Pascut, H. T. Goh, N. Welch, L. D. Buttery, C. Denning, and I. Notingher, Biophys J **100**, 251–259 (2011).
[15] A. Downes, R. Mouras, P. Bagnaninchi, and A. Elfick, J Raman Spectrosc **42**, 1864–1870 (2011).
[16] C. Aksoy and F. Severcan, Spectrosc-Int J **27**, 167–184 (2012).
[17] I. Notingher, I. Bisson, A. E. Bishop, W. L. Randle, J. M. P. Polak, and L. L. Hench, Anal Chem **76**, 3185–3193 (2004).
[18] L. L. McManus, G. A. Burke, M. M. McCafferty, P. O'Hare, M. Modreanu, A. R. Boyd, and B. J. Meenan, Analyst **136**, 2471–2481 (2011).
[19] G. Binnig, C. F. Quate, and C. Gerber, Phys Rev Lett **56**, 930–933 (1986).
[20] L. S. Dorobantu and M. R. Gray, Scanning **32**, 74–96 (2010).
[21] M. McElfresh, E. Baesu, R. Balhorn, J. Belak, M. J. Allen, and R. E. Rudd, P Natl Acad Sci USA **99**, 6493–6497 (2002).
[22] Y. Z. Wu, T. Yu, T. A. Gilbertson, A. H. Zhou, H. Xu, and K. T. Nguyen, Plos One **7** (2012).
[23] A. Pillarisetti, C. Keefer, and J. P. Desai, Springer Tracts in Advanced Robotics **54**, 261–269 (2009).
[24] A. Pillarisetti, J. P. Desai, H. Ladjal, A. Schiffmacher, A. Ferreira, and C. L. Keefer, Cell Reprogram **13**, 371–380 (2011).
[25] C. L. Keefer and J. P. Desai, Theriogenology **75**, 1426–1430 (2011).
[26] R. D. Gonzalez-Cruz, V. C. Fonseca, and E. M. Darling, P Natl Acad Sci USA **109**, E1523–E1529 (2012).
[27] R. Kiss, H. Bock, S. Pells, E. Canetta, A. K. Adya, A. J. Moore, P. De Sousa, and N. A. Willoughby, J Biomech Eng-T Asme **133** (2011).
[28] L. Blomberg, K. Hashizume, and C. Viebahn, Reproduction **135**, 181–195 (2008).
[29] P. L. Pfeffer and D. J. Pearton, Reproduction **143**, 231–246 (2012).
[30] C. E. Senner and M. Hemberger, Placenta **31**, 944–950 (2010).
[31] J. R. Hill, R. C. Burghardt, K. Jones, C. R. Long, C. R. Looney, T. Shin, T. E. Spencer, J. A. Thompson, Q. A. Winger, and M. E. Westhusin, Biology of Reproduction **63**, 1787–1794 (2000).
[32] F. Constant, M. Guillomot, Y. Heyman, X. Vignon, P. Laigre, J. L. Servely, J. P. Renard, and P. Chavatte-Palmer, Biology of Reproduction **75**, 122–130 (2006).
[33] P. Chavatte-Palmer, S. Camous, H. Jammes, N. Le Cleac'h, M. Guillomot, and R. S. F. Leed, Placenta **33**, S99–S104 (2012).
[34] P. W. Dyce, H. Zhu, J. Craig, and J. Li, Biochem Bioph Res Co **316**, 651–658 (2004).
[35] I. N. Sneddon, International Journal of Engineering Science **3**, 47–57 (1965).
[36] H. J. Butt, B. Cappella, and M. Kappl, Surf Sci Rep **59**, 1–152 (2005).
[37] M. J. Rosenbluth, W. A. Lam, and D. A. Fletcher, Biophys J **90**, 2994–3003 (2006).
[38] H. G. Schulze, S. O. Konorov, N. J. Caron, J. M. Piret, M. W. Blades, and R. F. B. Turner, Anal Chem **82**, 5020–5027 (2010).
[39] J. W. Chan, D. K. Lieu, T. Huser, and R. A. Li, Anal Chem **81**, 1324–1331 (2009).
[40] I. Notingher, S. Verrier, S. Haque, J. M. Polak, and L. L. Hench, Biopolymers **72**, 230–240 (2003).
[41] S. O. Konorov, C. H. Glover, J. M. Piret, J. Bryan, H. G. Schulze, M. W. Blades, and R. F. B. Turner, Anal Chem **79**, 7221–7225 (2007).
[42] G. J. Puppels, F. F. M. Demul, C. Otto, J. Greve, M. Robertnicoud, D. J. Arndtjovin, and T. M. Jovin, Nature **347**, 301–303 (1990).
[43] S. O. Konorov, H. G. Schulze, N. J. Caron, J. M. Piret, M. W. Blades, and R. F. B. Turner, J Raman Spectrosc **42**, 576–579 (2011).
[44] Y. Tan, S. O. Konorov, H. G. Schulze, J. M. Piret, M. W. Blades, and R. F. B. Turner, Analyst **137**, 4509–4515 (2012).
[45] L. Harkness, S. M. Novikov, J. Beermann, S. I. Bozhevolnyi, and M. Kassem, Stem Cells Dev **21**, 2152–2159 (2012).
[46] K. Asanoma, M. A. Rumi, L. N. Kent, D. Chakraborty, S. J. Renaud, N. Wake, D. S. Lee, K. Kubota, and M. J. Soares, Dev Biol **351**, 110–119 (2011).
[47] I. C. Scott, L. Anson-Cartwright, P. Riley, D. Reda, and J. C. Cross, Mol Cell Biol **20**, 530–541 (2000).
[48] B. B. McConnell, A. M. Ghaleb, M. O. Nandan, and V. W. Yang, Bioessays **29**, 549–557 (2007).
[49] R. Moll, Veroff Pathol **142**, 1–197 (1993).